water

MDPI

Article

Optimization of Advance Drainage Borehole Layout Based on Visual Modflow

Yue Li [1,*], Yunpeng Zhang [1], Yajie Ma [1] and Fangang Meng [2]

[1] College of Mining Engineering, North China University of Science and Technology, 21 Bohai Avenue, Caofeidian New Town, Tangshan 063210, China; mengf147852@126.com (Y.Z.); myj147852@126.com (Y.M.)
[2] Donghuantuo Mining Branch of Kailuan Group, Tangshan 063210, China; mengfangang@kailuan.com.cn
* Correspondence: 147@stu.ncst.edu.cn

Abstract: It is an effective measure to prevent water damage in coal mines in order to construct drainage boreholes in water-filled aquifers of a working face roof. The hydrogeological parameters of the roof water-filled aquifer and the parameters of the drainage borehole are closely related to the underground drainage effect. Taking the 3085 working face of the Donghuantuo Mine in Kailuan as an example, the influence degree of hydrogeological parameters and hydrophobic borehole parameters on the amount of drainage water was analyzed using the generalized gray correlation degree. Based on Visual Modflow, the 3D groundwater visualization model was established and the dredging borehole was generalized into the pumping borehole. By changing the main influencing factors, the design optimization of the advanced hydrophobic borehole was discussed. The results showed that the aquifer thickness had a great influence on the amount of water discharged, and the influence degree of the sharp angle between the formation and the direction of drilling, the depth of the final hole, the azimuth angle of drilling, the dip angle of drilling, the elevation of the final hole and the elevation of the borehole on the amount of water discharged decreased successively. Based on the simulation calculation, it could be observed that the hydrophobic borehole should be placed in a position with a larger accumulated thickness of the aquifer to have a better effect of hydrophobic depressurization.

Keywords: hydrophobic drilling; hydrogeological parameters; drilling parameters; Visual Modflow

Citation: Li, Y.; Zhang, Y.; Ma, Y.; Meng, F. Optimization of Advance Drainage Borehole Layout Based on Visual Modflow. *Water* **2024**, *16*, 2613. https://doi.org/10.3390/w16182613

Academic Editors: Zongjun Gao and Jiutan Liu

Received: 26 July 2024
Revised: 1 September 2024
Accepted: 6 September 2024
Published: 14 September 2024

1. Introduction

Coal mine water disasters seriously threaten the safe production of a mining area. At present, China's mine water prevention and control work adopts comprehensive control measures of prevention, plugging, dredging, drainage and interception [1]. According to the Detailed Rules for Coal Mine Water Prevention and Control, in order to realize the safe discharge of water inflow after mining, it is necessary to adopt advanced drainage measures for the fractured aquifer of the coal mine roof [2]. The commonly used method of hydrophobic depressurization is to construct drainage boreholes underground [3]. Drainage borehole water inflow, aquifer water pressure and water storage can directly evaluate the effect of borehole drainage. At present, the point source and line sink theory is mostly adopted for the calculation of drainage water from coal seam roof boreholes, but the flow pattern characteristics in the drainage holes are more complex, and the water amount calculation is not accurate enough [4–7]. Many scholars have analyzed the influence of borehole design parameters and roof aquifer hydrogeological parameters on the advance drainage effect using correlation analysis, gray correlation degree analysis, the single index model, the well flow calculation method, the numerical simulation method and other methods [8–13]. Taking the water drainage project of the Donghuantuo 3085 working face as an example,

the generalized gray relational degree analysis method is used to study the correlation between the aquifer hydrogeological parameters, drainage borehole parameters and drainage volume and determine the main influencing factors. Based on Visual Modflow, the groundwater flow field model of the pre-drainage of the working face was established, the main influencing factors were changed, the trend of the final water level of the aquifer under different drainage borehole distribution conditions was analyzed, the drainage capacity of the working face under different drainage schemes was summarized and the pre-drainage schemes were optimized.

2. Hydrogeological Survey of the Study Area

2.1. Water-Filled Aquifer

The coal measure strata and the Ordovician limestone strata at the bottom of Donghuantuo Mine are hidden under thick alluvium. In the mine field, the three-dimensional water-filling geological structure of the multi-layer aquifer with internal and external boundary communication is formed [14]. The 3085 working face is located in the central mining area. As the main mining coal seam of the working face, the water inflow of coal seam 8 mainly travels from the weak aquifer section (IVc) of coal seam 8 to coal seam 5 and the strong water-bearing section (Va+b) of coal seam 5.

Roof caving and fractures in coal seam mining destroy the roof aquiclude and lead to the upper aquifer. The range of the water-conducting fracture zone determines the range of the direct water-filling aquifer. The aquifer above the fracture zone also participates in the water inflow of the working face under the condition of natural vertical fracture communication [15]. The mining height of the coal seam in the 3085 working face is 2.9 m. The ratio of measured height to mining thickness in Donghuantuo Mine is 15.4, and the height of the roof water-conducting fracture zone is 46.2 m. Considering the upward conduction of natural vertical fracture development, the aquifer within the cumulative thickness of 100 m above coal seam 8 is used as the water source for roof filling. The hydrophobic borehole in the 3085 working face mainly drains the water above the roof of coal seam 5.

2.2. Arrangement of Drill Sockets and Hydrophobic Boreholes

The mining of coal seam 8 in Donghuantuo Mine of Kailuan has included a large number of drainage boreholes in the roof fractured aquifer in its construction, and the drainage boreholes have revealed the aquifer layer and its water-rich change [16]. A total of 12 drilling holes were laid on the 3085 working face, 7 drilling holes were laid on the air duct, and 5 drilling holes were laid on the haulage road. The specific distribution of the drilling holes is shown in Figure 1.

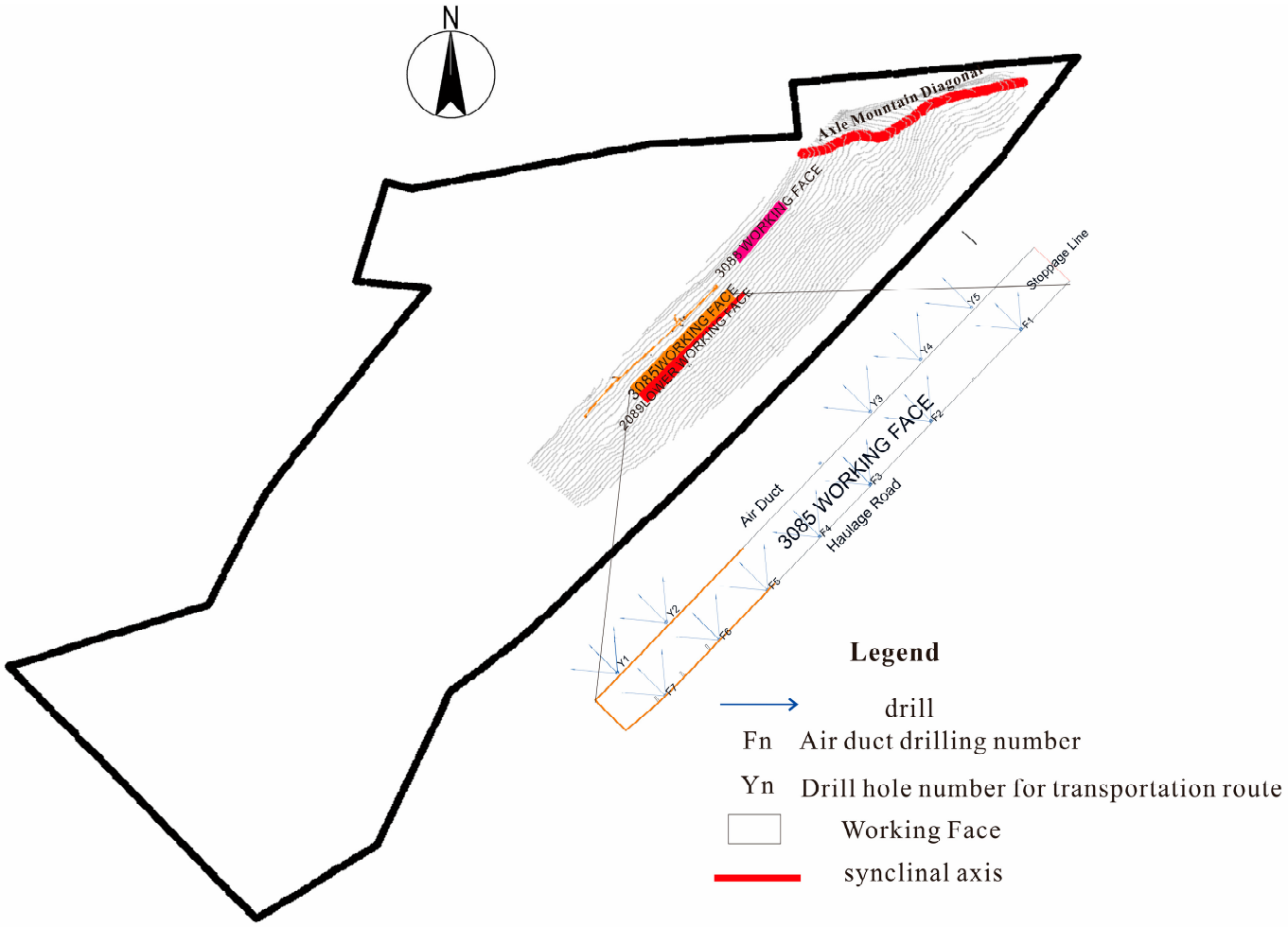

Figure 1. 3085 working face drainage borehole location diagram.

3. The Variation Law and Influencing Factors of Underground Borehole Drainage Water Quantity

3.1. Dynamic Variation Law of Borehole Water Inflow with Time

There is a matching and corresponding relationship between the dynamic water inflow of the advance drainage borehole and the hydrogeological conditions. By observing the dynamic water inflow of the borehole and analyzing the hydrogeological conditions of the working face, it can not only predict the degree of water damage but also determine whether it is suitable for mining. It is suitable for mining when the drilling water volume decreases rapidly or when the drilling water volume enters a stable period in a small case. If the amount of drilling water is large and does not drop continuously, additional drilling is needed to increase the intensity of drainage.

The dynamic curve of the water yield of the advance drainage borehole in the 3085 working face is illustrated in Figure 2. Taking Ss3085-1, Ss3085-2, Ss3085-3, Ss3085-19, Ss3085-20 and Ss3085-21 as examples, it can be seen from the figure that the initial water yield of boreholes Ss3085-1, Ss3085-2 and Ss3085-3 is large, but the decline rate is fast and the water yield of the boreholes is then kept at 0.1 m^3/min and enters a stable period. The water inflow of boreholes Ss3085-19, Ss3085-20 and Ss3085-21 remain at 0.05 m^3/min after three rapid declines. It can be observed that the borehole water inflow of the 3085 working face is a typical step-down type, and the initial water pressure of the working face is still high, with a stable supply.

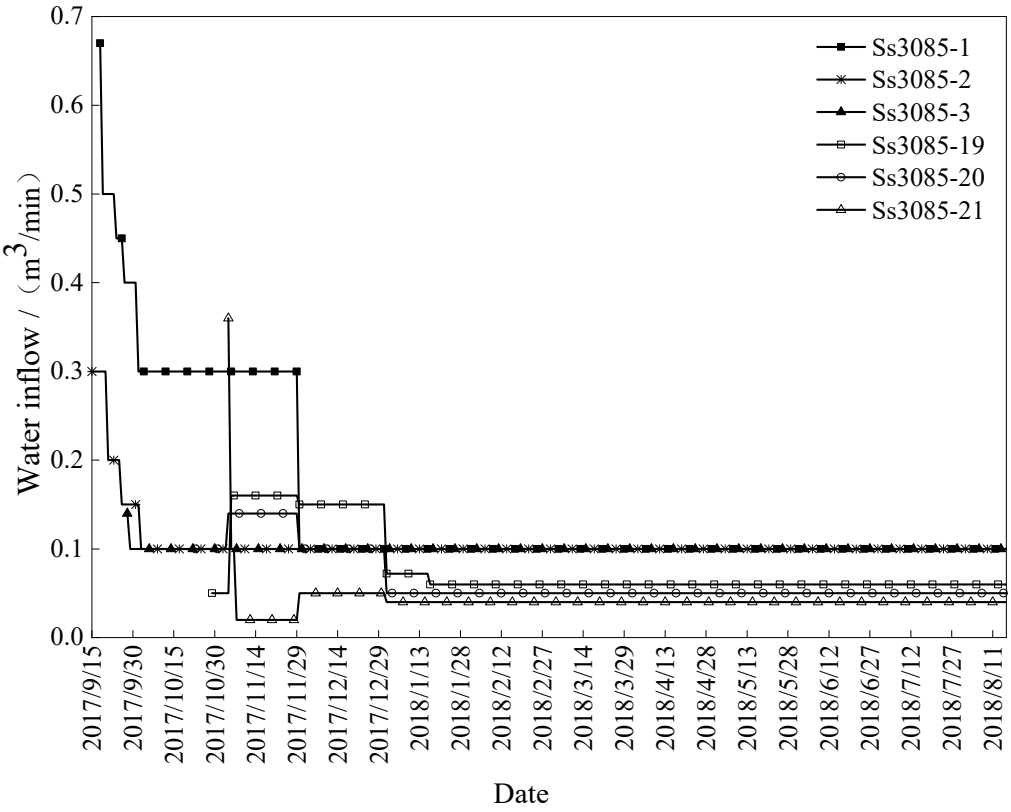

Figure 2. 3085 typical dynamic curve of drainage drilling in the working face.

3.2. Generalized Gray Correlation Analysis

Gray system theory is based on the similarity of the geometric shape of each factor to determine the degree of correlation between various factors. The generalized gray correlation degree combines the absolute gray correlation degree and the relative gray correlation degree and uses the area value between the two sequence curves to measure the similarity of the two sequence curves as a whole, which can analyze the correlation factors more comprehensively [17].

Absolute degree of gray incidence.

Let $X_i = (x_i(1),\ x_i(2),\ \cdots,\ x_i(n))$, be the sequence of system behavior, D_1 be the sequence of related factors.

$$X_iD_1 = (x_i(1)d_1,\ x_i(2)d_1,\ \cdots,\ x_i(n)d_1) \tag{1}$$

where $x_i(k)d_1 = x_i(k) - x_i(1)\ (k = 1, 2, \ldots, n)$ then D_1 is called the starting point annihilator, X_iD_1 is the starting point annihilator of X_i, denoted by:

$$X_iD_1 = X_i^0 = \left(x_i^0(1), x_i^0(2),\ \cdots,\ x_i^0(n)\right) \tag{2}$$

Assuming that the system behavior sequences X_i and X_j have the same length, they are both time-distance sequences, and their starting points are respectively:

$$X_i^0 = \left(x_i^0(1), x_i^0(2),\ \cdots,\ x_i^0(n)\right) \tag{3}$$

$$X_j^0 = \left(x_j^0(1), x_j^0(2),\ \cdots,\ x_j^0(n)\right) \tag{4}$$

$$|s_i| = \left|\int_1^n X_i^0 dt\right| = \left|\sum_{k=2}^{n-1} x_{i_i}^0(k) + \frac{1}{2}x_i^0(\mathrm{n})\right| \tag{5}$$

$$|s_j| = \left| \int_1^n X_j^0 dt \right| = \left| \sum_{k=2}^{n-1} x_j^0(k) + \frac{1}{2} x_j^0(\mathrm{n}) \right| \tag{6}$$

$$|s_i - s_j| = \left| \sum_{k=2}^{n-1} (x_{i_i}^0(k) - x_j^0) + (x_i^0(\mathrm{n}) - x_j^0(\mathrm{n})) \right| \tag{7}$$

The formula for calculating the gray absolute correlation degree is as follows:

$$\varepsilon_{ij} = \frac{1 + |s_i| + |s_j|}{1 + |s_i| + |s_j| + |s_i - s_j|} \tag{8}$$

Gray relative degree

Let $X_i = (x_i(1), x_i(2), \cdots, x_i(n))$ be the sequence of system behaviors, D_2 be the sequence of related factors.

$$X_i D_2 = (x_i(1)d_2, x_i(2)d_2, \cdots, x_i(n)d_2) \tag{9}$$

where, $x_i(k)d_2 = x_i(k)/x_i(1)$, $x_i(1) \neq 0 (k = 1, 2, \ldots, n)$, then D_2 is called the initializer, $X_i D_2$ is the initial image of X_i, denoted by:

$$X_i D_2 = X_i^{'} = \left(x_i^{'}(1), x_i^{'}(2), \cdots, x_i^{'}(n) \right) \tag{10}$$

The calculation formula of the gray relative correlation degree is as follows:

$$\gamma_{ij} = \frac{1 + |s_i'| + \left| s_j' \right|}{1 + |s_i'| + \left| s_j' \right| + \left| s_i' - s_j' \right|} \tag{11}$$

The gray comprehensive correlation formula is as follows:

$$\rho_{ij} = \theta \varepsilon_{ij} + (1 - \theta) \gamma_{ij} \tag{12}$$

ρ_{ij} is the gray comprehensive correlation degree between X_i and X_j, where $\theta \in [0, 1]$. Generally, $\theta = 0.5$.

3.3. Factors Affecting the Water Yield of the Hydrophobic Borehole

Taking the water yield of advanced drainage boreholes as the system characteristic sequence, the borehole orifice elevation, borehole orientation, borehole inclination, the final hole elevation, sharp angle between stratum and borehole direction, final hole depth and aquifer thickness are related factors. The seven influencing factors of the water discharge of the advanced drainage borehole are analyzed and calculated, and the results are shown in Table 1. (Please refer to the Supplementary Materials for drilling related data.)

Table 1. Generalized correlation analysis of influencing factors of drainage borehole water yield.

Influencing Factor	Gray Absolute Correlation Degree	Gray Relative Correlation Degree	Comprehensive Correlation Degree
The elevation of the borehole X_1 (m)	0.50005	0.50381	0.50193
The azimuth angle of drilling X_2 (°)	0.50015	0.53886	0.51951
The dip angle of drilling X_3 (°)	0.50041	0.50567	0.50304
The elevation of the final hole X_4 (m)	0.50006	0.50381	0.50194
The sharp angle between the formation and the direction of drilling X_5 (°)	0.50062	0.56743	0.53402
The depth of the final hole X_6 (m)	0.51283	0.52856	0.52069
The aquifer thickness X_7 (m)	0.50532	0.70263	0.60397

The gray absolute correlation degree is only applicable to the case where the dimensions of each variable are consistent or the magnitude changes little. For this study, the data of each main control factor are quite different, and the results may have errors; the gray relative correlation degree focuses on the degree of change of the representation relative to the starting point, which is also one-sided. The gray comprehensive correlation degree combines the characteristics of the two methods, and the results are more accurate. From the table, it can be seen that the gray comprehensive correlation degree of the influencing factors of the water discharge of the advanced drainage borehole is $X_7 > X_5 > X_6 > X_2 > X_3 > X_4 > X_1$, indicating that the aquifer thickness has a great influence on the amount of water discharged, and the influence degree of the sharp angle between the formation and the direction of drilling, the depth of the final hole, the azimuth angle of drilling, the dip angle of drilling, the elevation of the final hole and the elevation of the borehole on the amount of water discharged decreases successively.

4. Establish a Numerical Model of Groundwater Flow

Collect geological and hydrogeological data, establish a mathematical model of the groundwater system based on Modflow and simulate groundwater flow. In this model, the default groundwater density is a fixed value, and the differential equation for the three-dimensional unsteady flow of groundwater can be expressed as follows:

$$\frac{\partial H}{\partial t} = \frac{\partial}{\partial x}\left(K_{xx}\frac{\partial H}{\partial x}\right) + \frac{\partial}{\partial y}\left(K_{yy}\frac{\partial H}{\partial y}\right) + \frac{\partial}{\partial z}\left(K_{zz}\frac{\partial H}{\partial z}\right) + W \tag{13}$$

where K_{xx}, K_{yy}, K_{zz} are the permeability coefficients in the (x, y, z) directions (LT^{-1}), μ_s is the water storage rate (L^{-1}), H is the water head (L), t is time (T), W is the source sink term, with positive inflow and negative outflow (T^{-1}).

Based on the above generalization of aquifer and boundary conditions, a mathematical model for groundwater flow can be established as follows:

$$\begin{cases} \mu_s \frac{\partial H}{\partial t} = \frac{\partial}{\partial x}\left(K_{xx}\frac{\partial H}{\partial x}\right) + \frac{\partial}{\partial y}\left(K_{yy}\frac{\partial H}{\partial y}\right) + \frac{\partial}{\partial z}\left(K_{zz}\frac{\partial H}{\partial z}\right) + W & (x,y,z) \in \Omega \\ h(x,y,z) = h_0(x,y,z) & (x,y,z) \in \Omega \\ \left.\frac{\partial H}{\partial n}\right|_{\Gamma_i} = 0 \quad (i = 1,2,3,4) & (x,y,z) \in \Gamma \end{cases} \tag{14}$$

where $h_0(x, y, z)$ is the initial water head (L), Ω is the research area, Γ_i is the second type of boundary (waterproof boundary), i = 1, 2, 3, 4.

After investigating and analyzing the regional geological structure and hydrogeological conditions in the study area, the conceptual model and boundary conditions of groundwater movement in the study area are generalized, and the numerical model of groundwater flow is established.

4.1. Model Boundary Condition

The three-dimensional model of groundwater seepage based on Modflow requires a reasonable generalized boundary condition to describe the flow exchange between the study area and the surrounding environment [18]. There is water exchange around the simulation area, so it is considered the flow boundary, which is usually called the second boundary condition [19]. The Donghuantuo Mine is regarded as a typical mine with a developed inner boundary of planar fractures. Under the condition of vertical fracture communication in planar distribution, there is a certain hydraulic connection between the upper and lower water-bearing sections.

(1) Taking the 2089 lower working face as the shallow boundary, the 2089 lower face was completed in 2012. The study area of the coal seam 8 roof aquifer flows freely to the goaf of the haulage road, which is the constant head outflow boundary. The water

head value adopts the elevation value of the coal seam 8 floor and decreases from NE to SW.

(2) The −950 contour line of the coal seam 8 floor and the fault F18 are the deep boundaries. The coal seam 8 roof aquifer runs from NW to SE and is the mining area confluence. The boundary is the inflow boundary, which is far away from the mining area, and the groundwater level drops more evenly, which is the constant flow inflow boundary. The strike of the F18 fault is perpendicular to the direction of groundwater runoff. Depending on the understanding of 3D seismic exploration and production practice, most of the faults in the Donghuantuo Mine are transverse water-resisting faults, so the section of the F18 fault is the 0 flow boundary of water-resisting.

(3) The cutting hole along the formation trend line of the 3085 working face is used as the WS boundary. The boundary is basically consistent with the flow direction of groundwater, which is the inflow boundary with a small flow. However, there are few mining projects in the southern part of the boundary, the water level is higher than that in the study area, and the flow rate increases at the southern end.

(4) Taking the stop line of the 3085 working face along the stratigraphic dip line as the NE boundary, the northern area is a syncline axis and a steeply inclined wing, which is strongly affected by the 3088 working face and the north second mining area. The runoff direction is consistent with the boundary, which is a small flow boundary.

4.2. Generalization of Aquifer and Aquiclude

When the numerical method is used to establish the model, the aquifer group of coal measure strata is divided according to the stable development of the impermeable layer in the whole mining area [20]. The aquifer group contains multiple water-bearing layers and water-resisting layers, resulting in the insufficient accuracy of groundwater numerical model simulation. The lithology change of sedimentary strata can reflect the sedimentary environment. By comparing the stratification of borehole lithology, the aquifer and aquiclude can be divided in detail [21,22]. The lithology of the strata within 100 m above the roof of coal seam 8 in the 3085 working face mainly includes sandstone, siltstone, clay rock, shale and coal. Through a comparison of lithology, the roof of coal seam 8 in the study area is subdivided into 27 lithologic layers from bottom to top, as shown in Table 2. According to the comprehensive lithology, the water content and impermeability of each layer are determined. The strong aquifer represents the lithology of medium coarse sandstone, mainly sandstone; the representative lithology of the aquifer is fine sandstone, fine sandstone with clay or siltstone; the weak permeable layer represents the lithology of siltstone and siltstone with clay rock; the representative lithology of the aquiclude is mainly clay rock and shale.

The main strong aquifers in the 3085 working face are seven layers, which are the 3rd, the 7th, the 14th, the 16th, the 20th, the 22nd and the 24th layers. The comprehensive thickness of the strong aquifers is 10.44~55.65 m, and the average thickness is 31.16 m. The 3rd layer and the 7th layer are near coal seam 8 and within the scope of the caving zone. The thicknesses of the 3rd layer and the 7th layer are thicker, and the local thickness is extra thick. The local thickness of the 3rd layer reaches 25.50 m, which is the maximum thickness of the strong aquifers. The average thickness of the 14th and 16th strong aquifers in the middle section are thicker. There are four layers of aquifers in the 3085 working face, which are the 5th, 10th, 13th and 26th layers. The comprehensive thickness of the aquifers is 2.90~19.80 m, and the average thickness is 10.18 m. The average thickness of the 5th aquifer near coal seam 8 is thicker and uniform. There are 10 layers of weak permeables in the 3085 working face, which are the 2nd, 4th, 8th, 12th, 15th, 17th, 19th, 23rd, 25th and 27th layers. The comprehensive thickness is 19.72~52.95 m, and the average thickness is 40.39 m. The average thickness of the 2nd weak permeable layer near coal seam 8 is 2.02 m, and the thickness is quite different. There are six layers of aquicludes in the 3085 working face, which are the 1st layer, 6th layer, 9th layer, 11th layer, 18th layer and 21st layer. The comprehensive thickness is 2.80~35.50 m, and the average thickness is 19.32 m. The average

thickness of the 6th aquiclude near coal seam 8 is thicker. The average thickness of the 6th aquiclude is 5.33 m, and the local thickness can reach 22.53 m. The 3rd strong aquifer, the 5th strong aquifer and the 7th strong aquifer are the main water filling layers of coal seam 8, and the water source above the roof of coal seam 8 is abundant.

Table 2. Characteristics of aquifer thickness in model area.

Level Number	Comprehensive Lithology	Average Thickness/m	Maximum Thickness/m
The 24th strong aquifer layer	Medium sandstone and fine sandstone	2.86	8.30
The 22nd strong aquifer layer	Sandstone with a small amount of siltstone	2.00	10.20
The 20th strong aquifer layer	Sandstone with a small amount of siltstone	3.30	7.35
The 16th strong aquifer layer	Medium sandstone and fine sandstone	6.33	20.47
The 14th strong aquifer layer	Medium sandstone and fine sandstone	6.26	27.21
The 7th strong aquifer layer	Medium sandstone and fine sandstone	5.52	13.30
The 3rd strong aquifer layer	Medium sandstone and fine sandstone	4.88	25.50
The 26th aquifer layer	Fine sandstone	1.41	5.28
The 13th aquifer layer	Fine sandstone with a small amount of clay or siltstone	3.08	8.70
The 10th aquifer layer	Fine sandstone	0.46	2.80
The 5th aquifer layer	Fine sandstone	5.23	10.83
The 27th weak permeable layer	Siltstone with mudstone	4.37	10.30
The 25th weak permeable layer	Siltstone with mudstone	7.51	22.59
The 23rd weak permeable layer	Siltstone with mudstone	1.35	6.40
The 19th weak permeable layer	Siltstone with coal or clay	3.13	10.77
The 17th weak permeable layer	Siltstone	1.57	8.39
The 15th weak permeable layer	Siltstone with coal	1.59	10.98
The 12th weak permeable layer	Siltstone	3.62	11.30
The 8th weak permeable layer	Siltstone	11.65	22.80
The 4th weak permeable layer	Siltstone	3.57	11.60
The 2nd weak permeable layer	Siltstone	2.02	5.50
The 21st aquiclude layer	Siltstone with clay	3.50	25.80
The 18th aquiclude layer	Coal and clay	1.11	6.98
The 11th aquiclude layer	Coal and clay	1.55	8.25
The 9th aquiclude layer	Coal and clay	5.50	20.75
The 6th aquiclude layer	Coal and clay	5.32	22.53
The 1st aquiclude layer	Coal and clay	2.33	11.36

4.3. Establishment of Geometric Model

Using the finite difference method, the simulation area is divided into several cells of 40 m × 40 m by rectangular subdivision, which is divided into 60 grids in the X direction and 58 grids in the Y direction.

The fault structure in the study area is relatively developed, and the existence of faults will affect the safety of coal mining. Affected by the fault structure, the coal seam floor strata are broken and moved, and the water-conducting fissures in the aquiclude increase, which reduces the water-resisting ability of the aquiclude and increases the risk of water inrush from the coal seam floor. The fault intensity index is the total of the product of the drop of all faults per unit area and its strike length, which can reflect the complexity of faults in the study area. The greater the fault intensity index, the stronger the risk of water inrush from the coal seam floor. The distribution of the fault intensity index is shown in Figure 3. Import the elevation data into the model to assign the elevation of each layer to generate a three-dimensional model, as shown in Figure 3. Different aquifers and impermeable

layers are set with different colors, and each layer is generalized into a complete stratum in the simulation area without stratum loss. In the 3085 working face, 12 drilling holes and 32 drainage holes were constructed. The hydrophobic borehole of the same drilling socket is generalized into the same pumping well. The position of the well is determined by the final hole position of the borehole, and the position of the casing is penetrated from the elevation of the final hole to the model floor. All the casings penetrate the strata below the 10th aquifer; some penetrate the 14th aquifer, the 16th aquifer and the 20th aquifer; and a few penetrate the 22nd aquifer. The distribution of aquifers, aquicludes and wells in the model is shown in Figure 4.

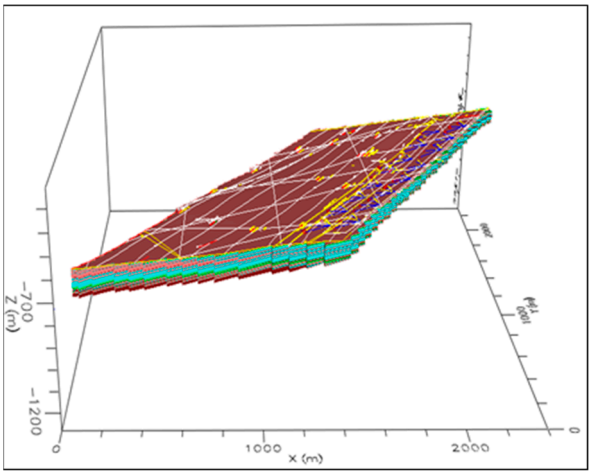

Figure 3. Schematic diagram of geometric model with a 1:1 horizontal longitudinal ratio.

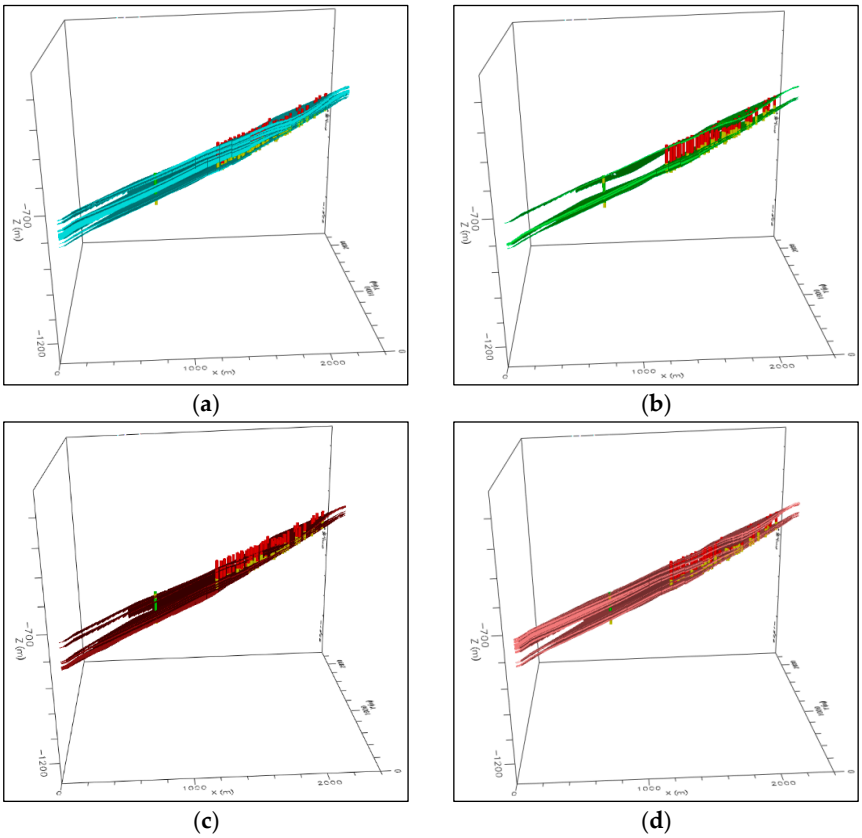

Figure 4. Three-dimensional model aquifer and well display diagram. (**a**) Strong aquifer layers. (**b**) Aquifer layers. (**c**) Weak permeable layers. (**d**) Aquiclude layers.

The 3D model of the coal seam 8 floor contour line is fitted with the actual coal seam 8 floor contour map. The fitting results are shown in Figure 5. The lowest elevation of the simulation area is −950 m, the highest is −500 m and the contour interval is 50 m. It can be seen from the figure that the fitting effect is good, and the created 3D model is more realistic.

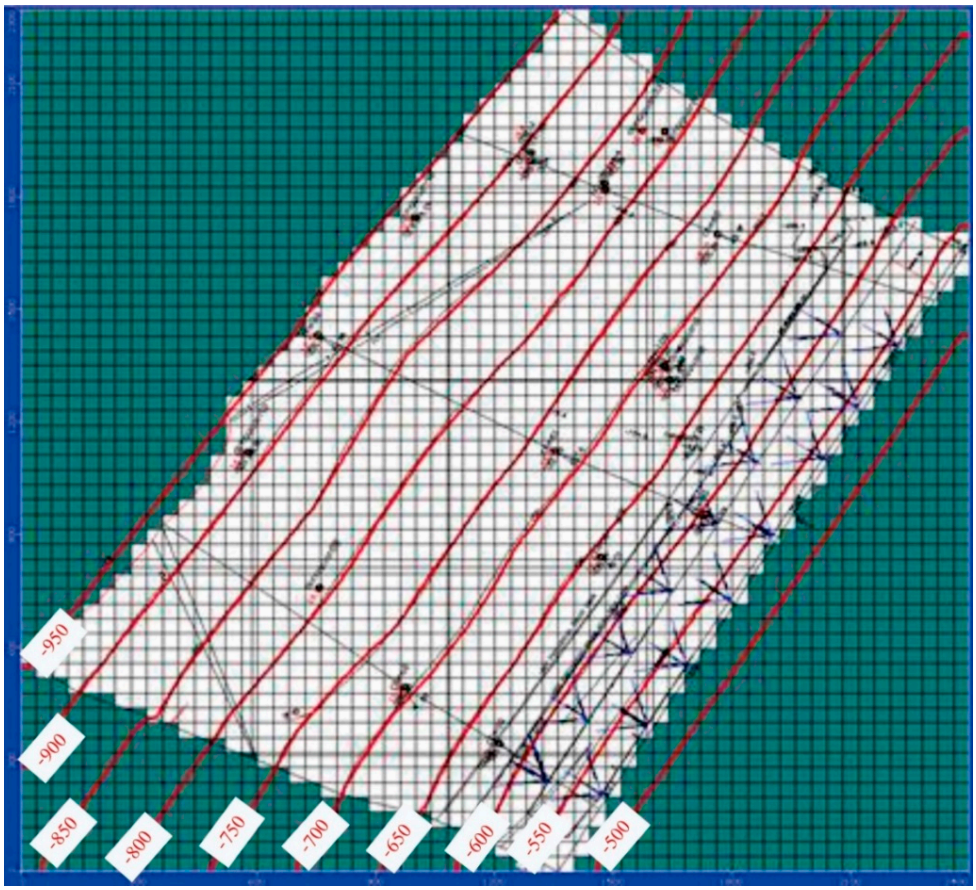

Figure 5. Elevation fitting result diagram of the coal seam 8 floor.

4.4. Model Identification and Verification

The identification of the model is also called model inversion. By continuously adjusting the hydrogeological parameters and equilibrium terms, the measured values of the groundwater level in the same period are fitted [23]. Ensure that the constructed model can more truly reflect the hydrogeological conditions of the simulation area and more reasonably describe the groundwater flow state. The model is identified by fitting the long-term hole water level data. Model validation was carried out after the model fitting. Keeping the parameters unchanged, the correctness of the model is judged by using the long-term observation data after the fitting period. There is a long view hole in Dongguan 55 in the 3085 working face. The curve of fitting calculation water level and actual change water level of the Dongguan 55 hole is shown in Figure 6. The water level change of the model is in good agreement with the actual situation; a suitable fitting recognition effect is achieved.

The calculated water level and observed water level values of the Dongguan 55 hole are shown in Table 3. The error between the simulated water level and the actual water level is mostly controlled within 5 m, with a maximum error of only 7.81 m. Using formula 13 to calculate the simulated water level error rate, the maximum error rate is only 1.63%, indicating a good simulation effect.

$$\text{Error rate} = \frac{|\text{Calculated water level} - \text{Observing water level}|}{\text{Observing water level}} * 100\% \quad (15)$$

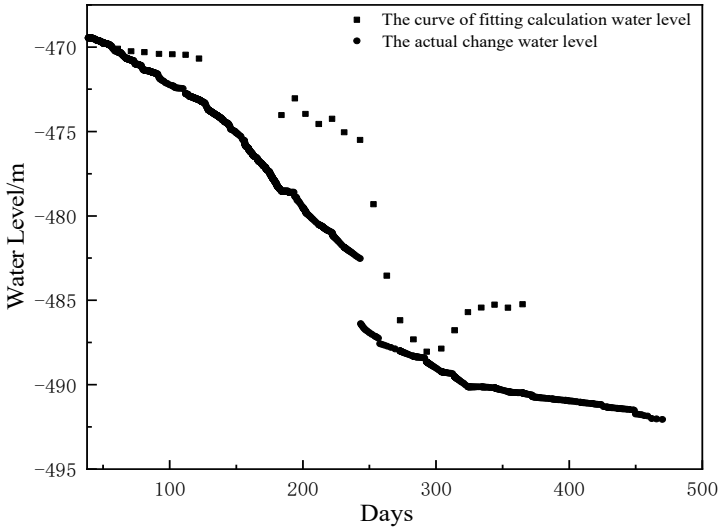

Figure 6. Dongguan 55 hole water level change fitting curve diagram.

Table 3. Table of simulated and measured water levels in the Dongguan 55 hole.

Observed Time	Observing Water Level/m	Calculated Water Level/m	Error Value/m	Error Rate
41	−469.47	−469.47	0.00	0.00
51	−469.82	−469.79	0.03	0.01
61	−470.1	−470.30	−0.20	0.04
71	−470.25	−470.77	−0.52	0.11
81	−470.3	−471.37	−1.07	0.23
92	−470.4	−471.81	−1.41	0.30
102	−470.43	−472.30	−1.87	0.40
112	−470.46	−472.77	−2.31	0.49
122	−470.68	−473.11	−2.43	0.52
184	−474.03	−478.54	−4.51	0.95
194	−473.04	−478.84	−5.80	1.23
202	−473.96	−479.72	−5.76	1.22
212	−474.56	−480.51	−5.95	1.25
222	−474.25	−481.00	−6.75	1.42
231	−475.05	−481.85	−6.80	1.43
243	−475.5	−482.52	−7.02	1.48
253	−479.31	−487.12	−7.81	1.63
263	−483.54	−487.72	−4.18	0.86
273	−486.19	−488.00	−1.81	0.37
283	−487.32	−488.31	−0.99	0.20
293	−488.05	−488.65	−0.60	0.12
304	−487.86	−489.23	−1.37	0.28
314	−486.78	−489.51	−2.73	0.56
324	−485.71	−490.11	−4.40	0.91
334	−485.43	−490.13	−4.70	0.97
344	−485.26	−490.18	−4.92	1.01
354	−485.44	−490.41	−4.97	1.02
365	−485.24	−490.48	−5.24	1.08

5. Simulation and Optimization of Advance Drainage Borehole Layout

The layout of advanced drainage boreholes in the roof of the 3085 working face was optimized to reduce the number of drainage boreholes and reduce the drainage time. Through gray correlation analysis, it can be seen that the thickness of the aquifer has a

great influence on the water output of the advanced drainage borehole. Combined with the data of drainage boreholes, the total thicknesses of all aquifers and strong aquifers from the 3rd layer to the 16th layer of the 3085 working face are counted. The total thickness contour map of the roof aquifer of coal seam 8 is shown in Figure 7. The total thickness of the aquifer is more than 7 m, and the local thickness can reach 21 m.

A total of 12 drainage points were arranged in the 3085 working face, of which seven drainage points were arranged on the air duct, namely F1, F2, F3, F4, F5, F6 and F7. Five hydrophobic points were arranged on the haulage road, namely Y1, Y2, Y3, Y4 and Y5. It can be seen from Figure 7 that the F2 drainage point and the F4 drainage point are in the weak area of the roof aquifer thickness. Considering the thickness of the aquifer and the principle of uniform pore distribution, the F2 drainage point and the F4 drainage point are moved to the B1 drainage point and the B2 drainage point, respectively. The drainage project of the original drainage point position is cancelled, and the same drainage work is set at the moved drainage point position as the original drainage point, and the influence of the two groups of drainage projects on the aquifer water level is compared.

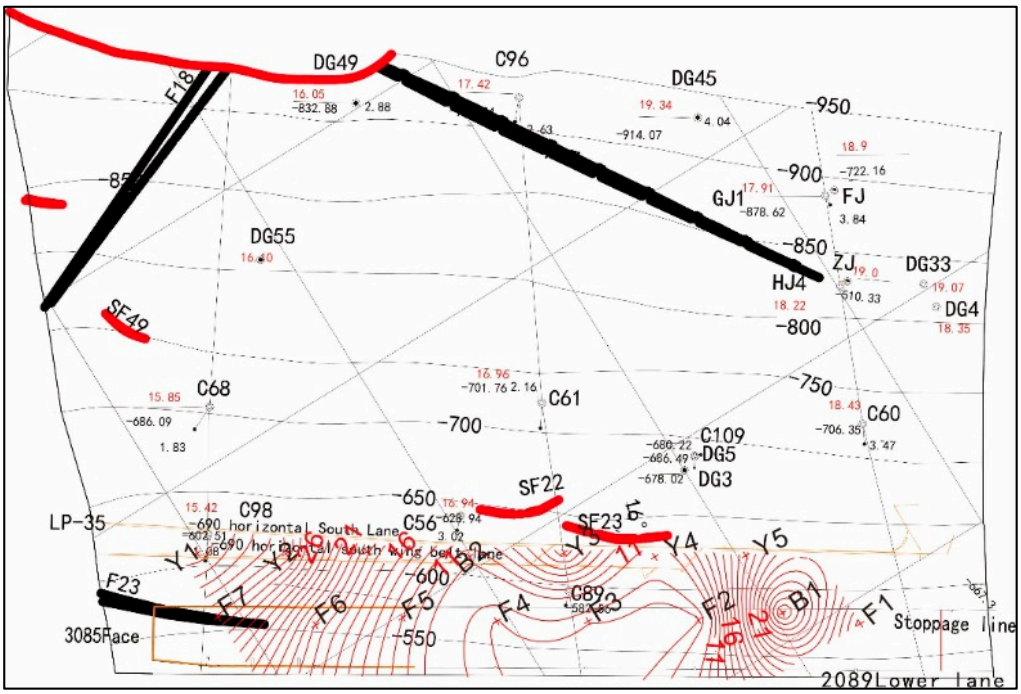

Figure 7. Contour map of the total thickness of the roof aquifer.

The day before the mining work, the water level line of the aquifer before and after the drilling optimization is illustrated in Figure 8. The water level at F1 is −460 m before optimization, and the water level at F1 is reduced to −465 m after optimization. After moving the hydrophobic point, the aquifer water level drops faster. Through numerical simulation, it can be observed that the drainage boreholes set at the larger cumulative thickness of the aquifer in the drainage layer can indeed carry out the roof advance drainage work more quickly.

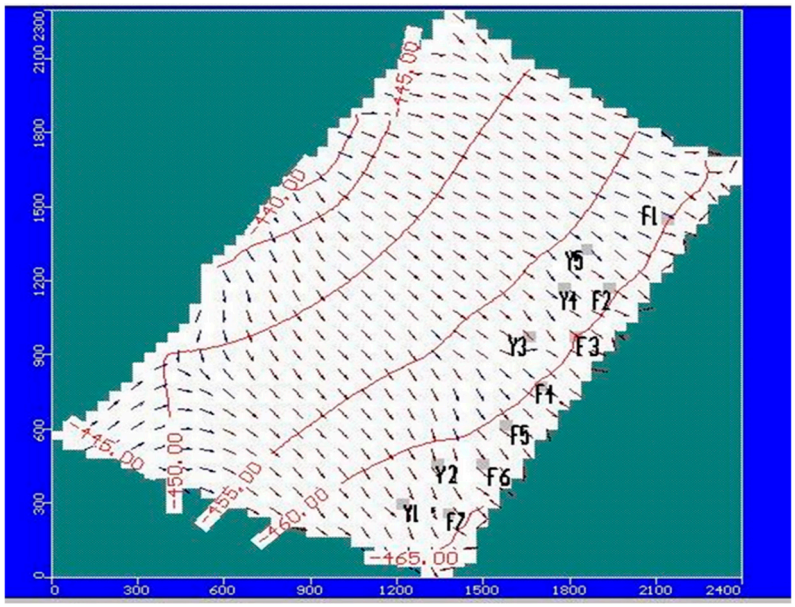

(**a**)

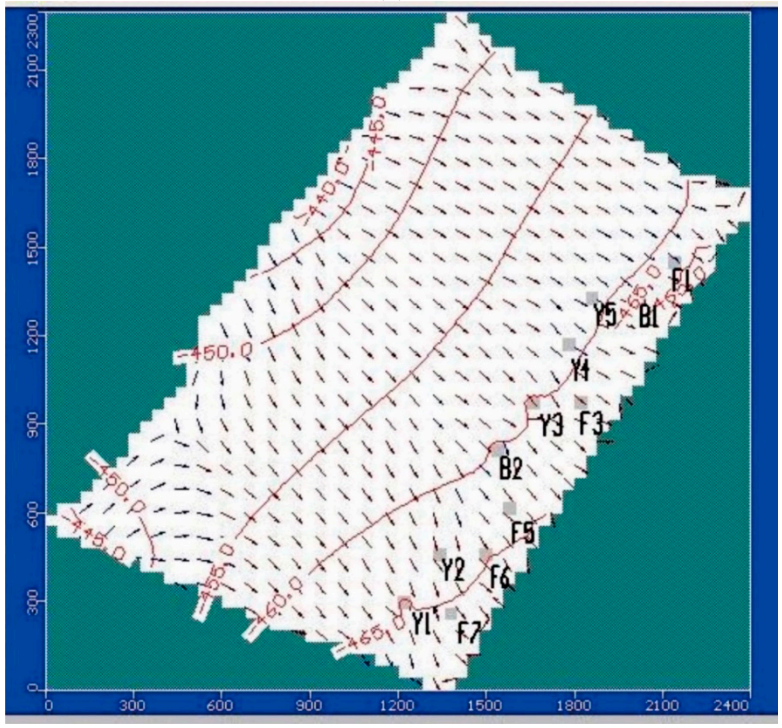

(**b**)

Figure 8. Distribution position and isoline diagram of aquifer drain hole. (**a**) Before optimization. (**b**) After optimization.

6. Conclusions

The gray comprehensive correlation method was used to analyze the factors affecting the water output of advanced drainage boreholes. The gray comprehensive correlation ranking of each influencing factor suggests that the main influencing factor on the water output of advanced drainage boreholes is the thickness of the aquifer.

The water source for filling the roof of the 3085 mining face is the aquifer within a cumulative thickness range of 100 m above the 8th coal seam. According to the lithology, it can be divided into 27 layers from bottom to top, with a total of 7 strong aquifers mainly composed of coarse to medium sandstone and 4 aquifers mainly composed of fine sand

and siltstone. The roof water source of this working face is abundant, and pre-drainage is required before mining.

Comparing the calculated water level and observed water level data of the Dongguan 55 hole, the two sets of values are relatively close with a small error rate. It is believed that the three-dimensional model of groundwater seepage established based on Visual Modflow numerical simulation software is in line with the actual water level dynamics and can optimize the advanced drainage drilling layout plan. Comparing the models before and after optimization, the layout of advanced drainage boreholes should fully consider the development range of the roof conductivity and the hydrogeological conditions of the roof aquifer. When the drainage boreholes are set at locations with thicker roof aquifers, the effect of advanced drainage work is better.

Supplementary Materials: The following supporting information can be downloaded at: https://www.mdpi.com/article/10.3390/w16182613/s1, Table S1: Drilling data.

Author Contributions: Conceptualization, Y.L. and Y.M.; methodology, Y.L.; software, Y.L.; validation, Y.L., Y.M. and Y.Z.; formal analysis, Y.L.; investigation, F.M.; resources, F.M.; data curation, Y.M.; writing—original draft preparation, Y.L.; writing—review and editing, Y.Z.; visualization, Y.L.; supervision, Y.M.; project administration, F.M.; funding acquisition, Y.L. All authors have read and agreed to the published version of the manuscript.

Funding: This paper did not receive funding support.

Data Availability Statement: All data, models, or code generated or used during the study are available from the corresponding author by request.

Acknowledgments: The authors would like to sincerely thank the Donghuantuo Coal Mine of Kailuan Group for providing the geological data.

Conflicts of Interest: Author Fangang Meng was employed by the company Donghuantuo Mining Branch of Kailuan Group. The remaining authors declare that the research was conducted in the absence of any commercial or financial relationships that could be construed as a potential conflict of interest.

References

1. State Administration of Coal Mine Safety. *Detailed Rules for Coal Mine Water Prevention and Control*; China Coal Industry Publishing House: Beijing, China, 2018.
2. State Administration of Coal Mine Safety. *Regulations on Water Control in Coal Mines*; China University of Mining and Technology Publishing House: Xuzhou, China, 2009; p. 123.
3. Wu, Q. Progress, problems and prospects of prevention and control technology of mine water and reutilization in China. *J. China Coal Soc.* **2014**, *39*, 795–805. [CrossRef]
4. Chen, S.; Dong, S.; Li, J.; Wang, H.; Yang, J. Analytical solution for slanted well in the roof of coal mine working face. *J. China Coal Soc.* **2016**, *41*, 1517–1523. [CrossRef]
5. Wang, G.; Liu, B.; Li, Y. Analysis on Prediction Method of Water Inflow of Drilling Hole in Mailing Underground Drilling. *Coal Technol.* **2019**, *38*, 96–98. [CrossRef]
6. Zhan, H.; Cao, J. Analytical and semi-analytical solutions of horizontal well capture times under no-flow and constant-head boundaries. *Adv. Water Resour.* **2000**, *23*, 835–848. [CrossRef]
7. Zhan, H.; Wang, L.V.; Park, E. On the horizontal-well pumping tests in anisotropic confined aquifer. *J. Hydrol.* **2001**, *252*, 37–50. [CrossRef]
8. Zheng, Y.; Ma, Y.; Zhang, C. Water drainage law in No.8 coal seam roof of Donghuantuo Coal Mine. *Coal Eng.* **2017**, *49*, 67–70.
9. Zhao, B. Application of gray correlation in the effect analysis of underground drilling water drainage. *J. Liaoning Tech. Univ. (Nat. Sci.)* **2013**, *32*, 289–292.
10. Zhao, C.; Dong, S.; Wang, H.; Jin, D.; Li, C.; Wang, S.; Zhou, Z.; Liu, Y. Analysis of water inrush from boreholes for drainage of confined aquifer by upward boreholes in underground coal mining face. *J. China Coal Soc.* **2020**, *45*, 405–414. [CrossRef]
11. Zhou, Z. Application of the monoexponential decay function on analyzing water-inflow in underground boreholes. *J. Min. Saf. Eng.* **2018**, *35*, 642–648. [CrossRef]
12. Yang, Z.; Dou, L.; Liu, C.; Xu, M.; Lei, Z.; Yao, Y. Application of high-pressure water jet technology and the theory of rock burst control in roadway. *Int. J. Min. Sci. Technol.* **2016**, *26*, 929–935. [CrossRef]
13. Ma, Y.; Zuo, W.; Liu, B.; Gao, L.; Chang, J. Analysis on law of geological structures controlling groundwater in buried syncline nose:a case in the Donghuantuo Coal Mine, Kailuan. *J. China Coal Soc.* **2012**, *37*, 157–160. [CrossRef]

14. Guo, W.; Lou, G.; Zhao, B. Study on the height of water-conductive fracture zone in alternate overburden of soft and hard with top coal caving mining in Lugou coal mine. *J. Min. Saf. Eng.* **2019**, *36*, 519–526. [CrossRef]
15. Wang, F.; Wu, S.; Li, Y.; Meng, X.; Wang, Z. Tracing Design Method of Pectinate Directional Borehole of Tunnels in Underground Mine. *Saf. Coal Mines* **2017**, *48*, 153–156. [CrossRef]
16. Deng, J. *Grey System Theory Tutorial*; Wuhan University of Technology Publishing House: Wuhan, China, 1992.
17. Liu, S. *The Grey System Theory and Its Application*, 5th ed.; Science Publishing House: Beijing, China, 2010.
18. Ding, Y.; Ma, R.; Li, N. A simulation model for three-dimensional coupled wave-current flumes. *Eng. Mech.* **2015**, *32*, 68–74+88.
19. Li, X.; Li, Y.; Zhou, S. Study and Application of Forecasting System for Water Inrush Under High Pressure in Xiamen Submarine Tunnel Construction Based on GIS. *Procedia Environ. Sci.* **2011**, *10*, 999–1005. [CrossRef]
20. Wu, Q.; Dong, S.; Zhang, Z. *Water Hazard Prevention of Mine*; China University of Mining and Technology Publishing House: Xuzhou, China, 2007.
21. Shao, L.; Xu, X.; Wang, S.; Wang, D.; Gao, D.; Wang, X.; Lu, J. Research progress of palaeogeography and palaeoenvironmental evolution of coal-bearing series in China. *J. Palaeogeog Raphy (Chin. Ed.)* **2021**, *23*, 19–38. [CrossRef]
22. Lu, B.; Xiao, Y. Study on Lithological Division of Coal Bearing Fractured Aquifer in Heilongjiang Province. *J. Shandong Univ. Sci. Technol.* **2017**, *36*, 96–102. [CrossRef]
23. Thompson, K.; Cadle, S.; Roemer, G. Integrating Less Common Data Sources to Improve Groundwater Model Calibration. *Mine Water Environ.* **2015**, *34*, 153–161. [CrossRef]